



## Polyaspartic acid facilitates oxolation within iron(III) oxide pre-nucleation clusters and drives the formation of organic-inorganic composites

J. Scheck, M. Drechsler, X. Ma, M. T. Stöckl, J. Konsek, J. B. Schwaderer, S. M. Stadler, J. J. De Yoreo, and D. Gebauer

Citation: *The Journal of Chemical Physics* **145**, 211917 (2016); doi: 10.1063/1.4963738

View online: <http://dx.doi.org/10.1063/1.4963738>

View Table of Contents: <http://scitation.aip.org/content/aip/journal/jcp/145/21?ver=pdfcov>

Published by the AIP Publishing

---

### Articles you may be interested in

Polarization reversal in organic-inorganic ferroelectric composites: Modeling and experiment  
Appl. Phys. Lett. **107**, 142907 (2015); 10.1063/1.4932661

Terahertz and infrared transmission of an organic/inorganic hybrid thermoelectric material  
Appl. Phys. Lett. **104**, 141912 (2014); 10.1063/1.4871316

Room temperature positive magnetoresistance via charge trapping in polyaniline-iron oxide nanoparticle composites

Appl. Phys. Lett. **103**, 032408 (2013); 10.1063/1.4815998

Improvement in open circuit voltage of MEHPPV - FeS<sub>2</sub> nanoparticle based organic inorganic hybrid solar cell

AIP Conf. Proc. **1512**, 704 (2013); 10.1063/1.4791232

Magnetic properties of Fe-doped organic-inorganic nanohybrids  
J. Appl. Phys. **93**, 6978 (2003); 10.1063/1.1556163

---

An advertisement for AIP Applied Physics Reviews. It features a blue and orange design with a central image of a molecular structure. The text "NEW Special Topic Sections" is prominently displayed in white. Below it, "NOW ONLINE" is written in yellow, followed by the title "Lithium Niobate Properties and Applications: Reviews of Emerging Trends". The AIP logo and the journal name "AIP Applied Physics Reviews" are also present.

# Polyaspartic acid facilitates oxolation within iron(III) oxide pre-nucleation clusters and drives the formation of organic-inorganic composites

J. Scheck,<sup>1</sup> M. Drechsler,<sup>2</sup> X. Ma,<sup>3</sup> M. T. Stöckl,<sup>4</sup> J. Konsek,<sup>1,a)</sup> J. B. Schwaderer,<sup>1,a)</sup>  
S. M. Stadler,<sup>1,a)</sup> J. J. De Yoreo,<sup>5,6</sup> and D. Gebauer<sup>1,b)</sup>

<sup>1</sup>Department of Chemistry, University of Konstanz, Universitätsstr. 10, Konstanz 78457, Germany

<sup>2</sup>Laboratory for Soft Matter Electron Microscopy, BIMF, University of Bayreuth, Universitätsstr. 30, 95440 Bayreuth, Germany

<sup>3</sup>Department of Chemistry, Idaho State University, Pocatello, Idaho 83201, USA

<sup>4</sup>Bioimaging Center, University of Konstanz, Universitätsstr. 10, Konstanz 78457, Germany

<sup>5</sup>Physical Sciences Division, Pacific Northwest National Laboratory, Richland, Washington 99352, USA

<sup>6</sup>Department of Materials Science and Engineering, University of Washington, Seattle, Washington 98195, USA

(Received 7 June 2016; accepted 15 September 2016; published online 3 October 2016)

The interplay between polymers and inorganic minerals during the formation of solids is crucial for biominerization and bio-inspired materials, and advanced material properties can be achieved with organic-inorganic composites. By studying the reaction mechanisms, basic questions on organic-inorganic interactions and their role during material formation can be answered, enabling more target-oriented strategies in future synthetic approaches. Here, we present a comprehensive study on the hydrolysis of iron(III) in the presence of polyaspartic acid. For the basic investigation of the formation mechanism, a titration assay was used, complemented by microscopic techniques. The polymer is shown to promote precipitation in partly hydrolyzed reaction solutions at the very early stages of the reaction by facilitating iron(III) hydrolysis. In unhydrolyzed solutions, no significant interactions between the polymer and the inorganic solutes can be observed. We demonstrate that the hydrolysis promotion by the polymer can be understood by facilitating oxolation in olation iron(III) pre-nucleation clusters. We propose that the adsorption of olation pre-nucleation clusters on the polymer chains and the resulting loss in dynamics and increased proximity of the reactants is the key to this effect. The resulting composite material obtained from the hydrolysis in the presence of the polymer was investigated with additional analytical techniques, namely, scanning and transmission electron microscopies, light microscopy, atomic force microscopy, zeta potential measurements, dynamic light scattering, and thermogravimetric analyses. It consists of elastic, polydisperse nanospheres, ca. 50–200 nm in diameter, and aggregates thereof, exhibiting a high polymer and water content. Published by AIP Publishing. [<http://dx.doi.org/10.1063/1.4963738>]

## I. INTRODUCTION

The numerous solid iron(III) (oxyhydr)oxides exhibit differing properties and are thus utilized in various applications, e.g., ion exchange, sorption, or catalysis.<sup>1–4</sup> They form via the hydrolysis of iron(III) ions, and concomitant and/or subsequent oxolation, e.g., condensation of the as-formed hydroxo-complexes, depending on the reaction parameters such as pH and temperature. In many experimental settings, cluster- and particle-based pathways have been observed for iron(III) oxide nucleation and growth.<sup>2,5–7</sup> In the early stages of iron(III) hydrolysis, small species in the size range of 1–4 nm occur. Such polymeric clusters aggregate to form the different crystalline materials.<sup>2,5,6,8</sup> It was recently proposed that iron(III) (oxyhydr)oxide precipitation in such cluster-based pathways can be described within the notions of the so-called pre-nucleation cluster (PNC) pathway.<sup>9</sup> In this model, in contrast to the classical nucleation picture,

thermodynamically stable, partly hydrolyzed iron(III) clusters constitute the earliest precursors, which are highly dynamic, i.e., change connectivity and structure on time scales typical for rearrangements in solution, and are thus considered equilibrium species—solutes—of the homogeneous solution. According to this hypothesis, the event of phase separation is characterized by a decrease in the dynamics of the PNCs, e.g., by the formation of additional or stronger internal bonds. Dynamics slower than those in the solution then render them a second, initially liquid phase, whereas the interfacial surface is characterized by the transition from high (mother liquid) to slow dynamics (dense liquid nanodroplet). Driven by the reduction of interfacial surface area, aggregation yields larger species, which ripen towards the final stable or kinetically stabilized solid-state structure. However, until recently, the speciation of PNCs in the iron(III) oxide system and the mechanism underlying the change in dynamics as a central event in phase separation have remained unknown; it was shown shortly that at low driving force for phase separation (i.e., pH < ~3.0 and iron concentrations in the lower mM regime), solute PNCs are clusters of  $\text{Fe}(\text{OH})^{2+}$ , i.e., olation polymers

a)J. Konsek, J. Schwaderer, and S. M. Stadler contributed equally to this work.

b)Author to whom correspondence should be addressed. Electronic mail: Denis.Gebauer@uni-konstanz.de

where the charge is most likely balanced by spectator ions.<sup>10</sup> Due to the lability of the bonds connecting the iron(III) centers,<sup>11</sup> the hydroxo-bridged olation PNCs are highly dynamic, and the phase separation event is based on the onset of oxolation; the formation of strong and hence much less dynamic oxo-bridges within olation PNCs is the key event underlying the molecular mechanism of iron(III) oxide nucleation.<sup>10</sup> Considering this, it is particularly interesting, if and how macromolecular additives interact with the stable solute PNCs and influence the onset of oxolation, and with it, the phase separation mechanism. It is known that polyaspartic acid (pAsp) interacts strongly with precursors, intermediates, and final phases in various mineral systems during their nucleation. It represents a very efficient nucleation inhibitor for calcium carbonate.<sup>12,13</sup> Furthermore, pAsp is known to stabilize polymer induced liquid precursors (PILPs) in the  $\text{CaCO}_3$  system, which offer great potential in bio-inspired materials chemistry.<sup>14,15</sup> Thus, the presence of PNCs in the iron(III) oxide system makes the investigation of the interactions with pAsp highly interesting, especially in comparison with the pAsp  $\text{CaCO}_3$  system. Indeed, in the case of iron oxides, it is known that additives, which can be spectator ions, small molecules, or macromolecules, have an impact on size, morphology, and phase identity of iron(III) (oxyhydr)oxides.<sup>3,4,16–19</sup> It is obvious that the addition of polymers with functional groups that can interact with single ions, complex solute precursors, intermediates, and solid phases will have an effect on the multistep precipitation process. While numerous sugars and some complexing anions such as phosphate, sulfate, or silicates retard the transformation of amorphous intermediates into crystals, other additives, e.g., oxalic acid, promote the formation of crystalline species.<sup>16,20–22</sup> Further roles of additives include the adsorption of precipitates to the additives, or the competition between organic additives and  $\text{Fe(OH)}_4^-$  as ligands for growth sites in nascent nuclei.<sup>3,16,23</sup> The polyanion polyacrylic acid (PAA) was observed to form gels by complexing mononuclear iron(III) chloro complexes.<sup>23</sup> It was argued that the polymer binds exclusively these monomeric  $\text{FeCl}^{2+}$  species by chelating them with two deprotonated carbonyl groups.<sup>23</sup> A comparison of the iron(III)-pAsp system with a similar case of  $\text{CaCO}_3$ -poly(styrene sulfonate) (PSS) seems promising for a more comprehensive understanding of general additive effects on precipitation in mineral systems. In the case of  $\text{CaCO}_3$ -PSS,  $\text{Ca}^{2+}$  ions were found to bind strongly to the additive, generating a localized critical supersaturation, finally inducing localized nucleation.<sup>24</sup> This relates to the above-mentioned iron(III)-(oxyhydr)oxide-PAA system,<sup>23</sup> suggesting that there might be common mechanism of polyelectrolyte additives influencing distinct mineral systems via the sequestration of single cations.

Studying the iron(III)-(oxyhydr)oxide-pAsp system is not only highly interesting to confirm or refute this hypothesis but also a detailed physical chemical understanding of the effects of polymeric additives on the iron oxide precipitation pathway during the pre-nucleation, nucleation, and post-nucleation stages has not been achieved, while it is a pre-requisite for the development of target-oriented synthetic strategies towards

the generation of iron oxides with advanced properties, and also new organic-inorganic hybrid materials. Such materials, so-called composites, are built up from both organic and inorganic components that are combined in one structure. Composite materials unite the properties of the soft and hard components and consequently exhibit properties that are distinct from those of the single constituents.<sup>25</sup> Due to their potential numerous applications, iron oxide-polymer composites are of high interest.<sup>23,26,27</sup>

The titration assay used in this study was specifically designed to investigate the early stages of iron(III) hydrolysis.<sup>10</sup> Herein, we demonstrate that it also yields information on the changes in the pathway induced by the addition of the polymer. Different analytical techniques were applied to characterize the resulting precipitation product, and complementary analyses enabled the characterization of the material properties. It turns out that the addition of the polymer delicately influences the iron(III) oxide precipitation pathway, driving the phase separation event, as opposed to its strong inhibitory effect in other mineral systems. Thus, we provide fundamental insight into the mode of influence of pAsp on the early stages of iron(III) oxide formation, highlighting that polyanions may be particularly promising additives for the generation of novel iron oxide-based composite materials in the future.

## II. EXPERIMENTAL

### A. General

All chemicals were used as received: iron(III) nitrate nonahydrate (Sigma Aldrich, puriss. p.a., ACS reagent,  $\geq 98.0\%$ ), iron(III) chloride hexahydrate (Sigma Aldrich, puriss. p.a., ACS reagent, 98%-102%), HCl (Merck, 0.1M), NaOH (Merck, 0.1M), NaCl (VWR, 99.9%), and  $\text{HNO}_3$  (Sigma Aldrich, puriss. p.a., reag. ISO, reag. Ph. Eur.,  $\geq 65\%$ ). The stock solutions of pAsp were obtained by dissolving commercial Baypure<sup>®</sup> DS100 ( $M_w = 1200 \text{ g/mol}$ ) and ( $M_w = 1500\text{--}3800 \text{ g/mol}$ ) in Milli-Q water. All solutions and dilutions were prepared with water of Milli-Q quality if not indicated otherwise.

### B. Titration assay

The hydrolysis was performed with an automated commercially available titration setup provided by Metrohm (Filderstadt, Germany). The titration device (836 Titrando) which operates two dosing units (800 Dosino) is operated with a commercial software (Tiamo 2.3) that controls the dosing of the solutions. The dosing units allow dosing volumes in increments as low as  $0.2 \mu\text{l}$  through burette tips, which are equipped with special valves preventing the diffusion of solution into (or out of) the titration reservoir. The pH values were measured utilizing an EtOH-Trode pH electrode (Metrohm, 6.0269.100). The electrode was calibrated regularly using three pH buffers (Mettler-Toledo) and the inner electrolyte, 3M KCl solution (Merck), was refilled before each titration. Turbidity measurements were

carried out using a spectrosense turbidity sensor (6.1109.110) equipped with a 610 nm laser. The titrations were performed at ambient temperature of  $(22 \pm 2)^\circ\text{C}$  in 100 ml beakers. After every titration, the glassware and the electrodes were cleaned with water of Milli-Q quality. In the titration experiments, a solution of 0.1M iron(III) chloride hexahydrate in 0.1M HCl was added at a rate of 0.01 ml/min into 30 ml of 0.01M HCl that was adjusted to the desired pH value by addition of the required amount of 0.05M NaOH prior to the titration. This pH value was kept constant throughout the titration by automatic counter titration of 0.05M NaOH solution.

### C. Titration in the presence of pAsp

Titrations in the presence of additives were carried out as described in Sec. II B, but prior to titration, the desired amount of a stock solution of 0.25 g/l pAsp or 2.5 g/l L-aspartic acid in water was added to the hydrochloric acid. The amount of pAsp was 0.05 g/l and pAsp with a molecular weight of 1500–3800 g/mol was used if not stated otherwise. Analysis of the composite material was carried out on samples drawn at 550 s from the titration at pH 2.5, corresponding to an iron(III) concentration between 0.26 and 0.3 mM if not stated otherwise. This point was chosen as, according to the turbidity measurements, the composite material of iron(III) oxide and pAsp is just forming and no precipitation or significant hydrolysis of surplus iron(III) ions is expected. It should be noted that without pAsp, the system is in the pre-nucleation equilibrium stage at this point, where no precipitation occurs (see Sec. III and in the [supplementary material](#)).

### D. Dynamic light scattering (DLS) and zeta potential measurements

Measurements of the zeta potential and of size distributions by DLS were carried out with a Zetasizer Nano ZS (Malvern Instruments).

### E. Atomic-force microscopy (AFM)

AFM images and force vs. distance measurements were obtained *in situ* with a Nanoscope VIII (Bruker) and oxide sharpened silicon nitride probes (PNP-TR,  $k = 0.32$  N/m, and tip radius  $< 10$  nm; NanoWorld) on samples drawn from the titrations after 4800 s, i.e., at an iron(III) concentration of 2.1–2.4 mM. These higher concentrations ensured that an adequate number of particles attached to mica surfaces on which the sample was placed for imaging. Samples containing only the polymer or obtained following titration in the absence of the pAsp were used as references.

### F. Isolation of the precipitate

The composite material was isolated for analyses from the titration assay. The solution was centrifuged with a preparative ultracentrifuge at 30 000 rpm for 45 min and the resulting sediment was freeze-dried.

### G. Electron microscopy

Scanning electron microscopy (SEM) measurements were performed with a Zeiss CrossBeam 1540XB, and transmission electron microscopy (TEM) images were recorded employing a JEOL JEM-2200FS microscope operating at 200 kV. The EDX spectra were obtained using a tabletop microscope TM 3000 (HITACHI). For cryo-TEM, samples drawn at an iron(III) concentration of 0.4 mM at pH 2.6 were spread and blotted with a filter paper on lacey carbon filmed copper grids. The resulting thin film was vitrified with liquid ethane at its freezing point by quickly plunging the grids into it. Specimens were examined at temperatures around 90 K with a Zeiss/LEO EM922 Omega TEM also operating at 200 kV. For constant enhancement, zero-loss filtered images were recorded at  $\Delta E = 0$  eV. Collected images were processed with a background-subtraction routine and, where appropriate, a smoothing filter was applied to reduce noise. In the titrations for *cryo*-TEM,  $\text{FeCl}_3 \times 6\text{H}_2\text{O}$  was replaced by  $\text{Fe}(\text{NO}_3)_3 \times 9\text{H}_2\text{O}$  and accordingly  $\text{HNO}_3$  instead of HCl was used.

### H. Thermogravimetric analysis (TGA) and XRD

TGA was performed in an oxygen atmosphere with a NETZSCH STA 449F3 Jupiter at a heating rate of 10 K/min and a sample mass of 5.585 mg. XRD diffraction patterns were collected utilizing a Bruker AXS D8 Advance diffractometer with a Göbelmirror PGM at a scan rate of 0.86 2θ/min using Cu  $\text{K}_\alpha$  radiation. To account for iron fluorescence, the data were background corrected.

### I. Light microscopy

The size of larger particle aggregates before and after rehydration was measured by light microscopy. Particles adsorbed on a glass substrate from solution ( $\mu$ -dish<sup>35 mm,high Glass Bottom, ibidi, Martinsried, Germany) were dried in a  $\text{N}_2$  stream and subsequently rehydrated in a water vapor saturated atmosphere. Transmitted light images using differential interference contrast of particles were recorded on a Zeiss Axio Observer, using a 100× (1.46 NA) oil immersion objective, a condenser set at 0.55 NA, and AxiocamMRm (Carl Zeiss Microscopy GmbH, Jena, Germany).</sup>

## III. RESULTS AND DISCUSSION

### A. Titration assay

A central objective of this work is the elucidation of the impact of pAsp on the precipitation pathway and its interaction with iron(III) (oxyhydr)oxide precursors. A titration setup providing slow mixing conditions at low pH and iron(III) concentrations was utilized to investigate the early species occurring during the iron(III) hydrolysis reaction with and without pAsp or monomeric L-aspartic acid. The different additives were dissolved in 0.01M HCl to yield a concentration of 0.05 g/l. Iron(III) chloride solution was then slowly added to each individual mixture, while the pH level

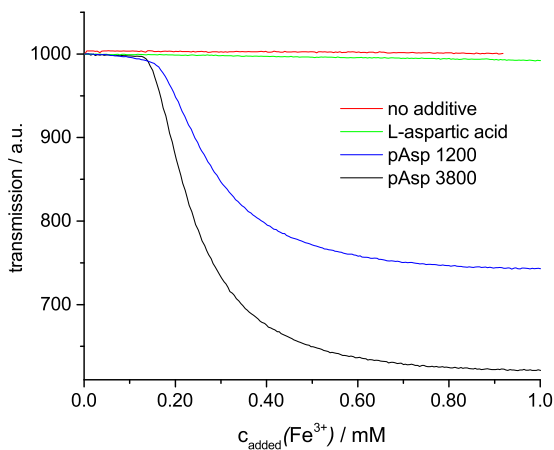


FIG. 1. Development of the transmission (arbitrary units, a.u.) of the reaction solution in a titration experiment with increasing iron(III) concentration. In the presence of pAsp, a distinct drop in transmission is observed that could not be detected for the same concentrations of the monomer L-aspartic acid or in the absence of additives. An increase in molecular weight leads to a more pronounced effect in the decrease of the transmission of the solutions. All additive concentrations were 0.05 g/l.

was kept constant. The titration with the same parameters but in the absence of additives served as a reference experiment. pAsp of two different molecular weights (1200 g/mol and 1500–3800 g/mol) as well as the monomer L-aspartic acid was investigated to explore the effects of polymer speciation, whereas also the effects of varying additive concentrations were assessed. The titration was carried out at pH 2.5, and the transmission of the reaction solution was monitored (Figure 1). In the presence of the polymers, a distinct increase in the turbidity of the reaction solution occurs at very low iron concentrations, which cannot be observed in the absence of the polymer, or in the presence of the monomer, L-aspartic acid (note that in the additive-free case, the solution is in a pre-nucleation equilibrium stage at this point, where the iron(III) concentration is very low, and iron oxides do not precipitate, see Figure S1 of the [supplementary material](#)). The sudden clouding of the reaction solution in the presence of pAsp indicates a phase separation event. This effect is more pronounced in case of the larger molecular weight of the polymer (Figure 1). In all cases, the mass concentration of the additives is the same and thus the number of moles of functional groups, so the mere presence of the functional groups at the given pAsp concentration does not cause any precipitation. Thus, it can be concluded that the chain length and possibly the structure of the polymer is crucial for the clouding and may relate to salting out.

In order to gain insight into the mechanism causing the very early onset of precipitation in presence of pAsp, as opposed to the reference experiment, the hydrolysis reaction was monitored with the titration assay: Throughout the titration experiment, the pH value was kept constant and the amount of NaOH solution that was required to maintain this constant pH value was recorded. The amount of hydroxide ions that is titrated for keeping the pH constant reflects the extent of the hydrolysis of iron(III), as the hydroxides are consumed by neutralization of the protons generated in this process. The polymer is protonated to more than 90% ( $pK_a = 3.65$ )<sup>28</sup> at this

pH level (i.e., between pH 2.0 and pH 2.7) and can thus be considered uncharged. As the concentration of the additive and thus of its functional groups was very low (approx. 0.4 mM carboxylic acid), the fraction of NaOH required for balancing any potentially occurring deprotonation of the polymer was negligible given the concentration of the added base (10 mM at pH 2.0 at 550 s).

In the absence of pAsp, no hydrolysis takes place at pH 2.0, and thus essentially no NaOH addition is required for keeping the pH constant, but with increasing pH, progressively more hydroxide ions are consumed and need to be replaced.<sup>10</sup> Figure 2 shows the molar ratio of reacted hydroxide ions (obtained from the base consumption) and added iron ions,  $\text{OH}^-/\text{Fe(III)}$ , in the presence of 0.05 g/l of pAsp 3800 at four different pH levels (pH 2.0, 2.3, 2.5, and 2.7). The comparatively large error bars at pH 2.0, where no hydrolysis takes place, derive from the counter titration of minor pH fluctuations caused by pH electrode tune-in, which gradually level off during later times of the experiment, i.e., the error bars become much smaller with proceeding time (thereby showing unambiguously that the extent of hydrolysis is negligible at pH 2.0<sup>10</sup>). At higher pH values, the amount of hydroxide ions that are consumed during hydrolysis becomes significant, and these pH changes lead to a much faster tune-in of the electrode signal, and thereby, smaller error bars are obtained already in the early stages of the experiments.

The progression of the  $\text{OH}^-/\text{Fe(III)}$  ratio (Figure 2) is a measure for the extent of iron(III) hydrolysis, even though it does not necessarily reflect the actual ratio in the formed material, as there is no information on the localization of reacted iron(III) ions: an unknown fraction of the added iron(III) ions can be present in the solution as dissolved and just partly hydrolyzed complexes, whereas the iron present in precipitates may be fully hydrolyzed. The reference experiments without pAsp show similar, constant, and low  $\text{OH}^-/\text{Fe(III)}$  ratios. At pH 2.0, also no  $\text{OH}^-$  is consumed (Figure 2(a)). With increasing pH, the  $\text{OH}^-/\text{Fe(III)}$  ratio increases to ~0.5 for pH 2.3 and pH 2.5 and up to 0.75 for pH 2.7, which can be assigned to an increasing extent of hydrolysis with increasing pH.<sup>10</sup> In the presence of pAsp, the dependency of the degree of hydrolysis on the pH value is even more pronounced, and the  $\text{OH}^-/\text{Fe(III)}$  ratio also differs significantly from the reference experiments, but only if hydrolysis occurs; there is no significant difference for the experiment at pH 2.0 in the presence and absence of pAsp within experimental error, and no precipitate is formed (Figure 3). At higher pH values and in the presence of pAsp, however, a different behavior can be observed. The  $\text{OH}^-/\text{Fe(III)}$  ratio increases in the beginning of the iron(III) addition up to a value of ~2, and then slowly drops to a lower level. This level becomes higher with increasing pH and ranges from ~0.5 at pH 2.3 to ~1.0 at pH 2.7 at 2000 s. The higher  $\text{OH}^-/\text{Fe(III)}$  ratio observed in presence of pAsp and at all investigated pH values higher than 2.3 is evidence for a direct influence of the polyanion on the progress of iron(III) hydrolysis. Interestingly, this is only the case if the pH-value of the solution is high enough for hydrolysis to take place and thus not observed for pH 2.0. Hence, it can be concluded that the reaction is facilitated by the additive and occurs at

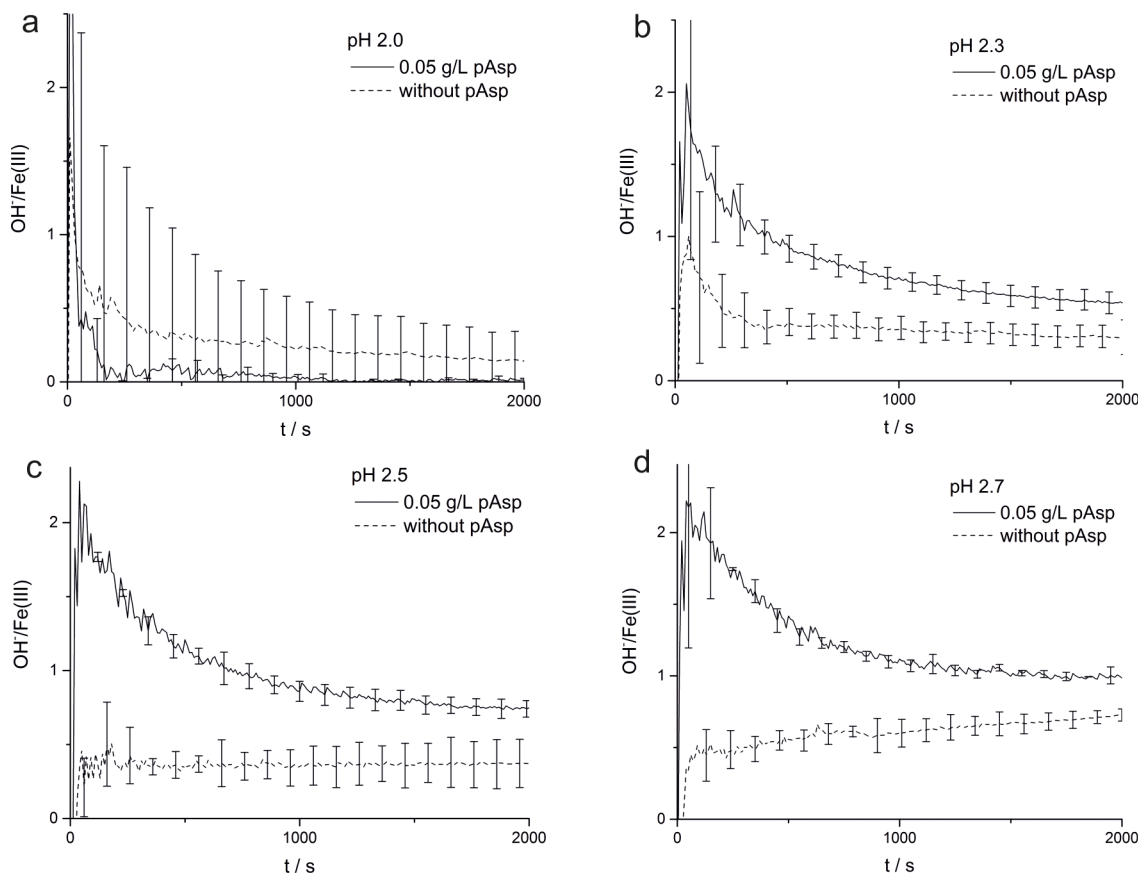


FIG. 2.  $\text{OH}^-/\text{Fe}(\text{III})$  ratio during hydrolysis at different pH values. The dotted lines represent the reference experiments, which do not contain additives, and the solid lines show titration data from hydrolysis in the presence of  $0.05 \text{ g/l}$  pAsp with a molecular weight of  $3800 \text{ g/mol}$ . (a) At pH 2.0, the curves show the same shape within the error bar while at (b) pH 2.3, (c) pH 2.5, and (d) pH 2.7, the  $\text{OH}^-/\text{Fe}(\text{III})$  ratio in the titration experiments with pAsp is significantly larger than in the reference experiments. The error bars display  $\pm(1-\sigma)$  standard deviations for  $2 \leq n \leq 7$  individual repetitions.

significantly lower iron(III) ion and hydroxide concentrations, i.e., lower pH values, than in the absence of the polymer. The presence of partly hydrolyzed species is fundamentally required for the effect to occur. Moreover, at a higher concentration of the additive, the observed effect becomes larger (see Figure S2 of the [supplementary material](#)). This suggests that the pAsp is used to capacity at this iron(III) concentration. Consistently, during the later stages of the experiment, the presence of the additive does not cause any significant effects, and the reactions with and without pAsp exhibit practically identical profiles upon ongoing addition of iron(III) solution (see Figure S3 of the [supplementary material](#)).

As monomeric L-aspartic acid does not show any hydrolysis promotion (Figure 1 and Figure S4 of the [supplementary material](#)), the influence of the molecular weight of pAsp was also examined. The maximum  $\text{OH}^-/\text{Fe}(\text{III})$  ratio is larger than 2.0 for pAsp 1500-3800, while it is around 1.25 for pAsp 1200. The level established during ongoing iron(III) addition, however, is approx. 1.0 for both polymers (see Figure S2 of the [supplementary material](#)). When the adsorption capacity of the polymer is saturated with inorganic species and iron(III) addition is continued, the  $\text{OH}^-/\text{Fe}(\text{III})$  ratio subsequently decreases. Consistently, an increase in pAsp concentration leads to an increase and broadening of the maximum  $\text{OH}^-/\text{Fe}(\text{III})$  ratio (see Figure

S2 of the [supplementary material](#)). Above pH 2.3 and with the same additive concentration, the maximum  $\text{OH}^-/\text{Fe}(\text{III})$  ratio is almost equal (Figure 2(b)). For different molecular weights, a correlation between the magnitude of the turbidity change upon hydrolysis and therefore between the amount of formed material and the maximum  $\text{OH}^-/\text{Fe}(\text{III})$  ratio is observed (Figures 1 and 2). Since this maximum is established very early on in the course of the experiment (Figure 2), this

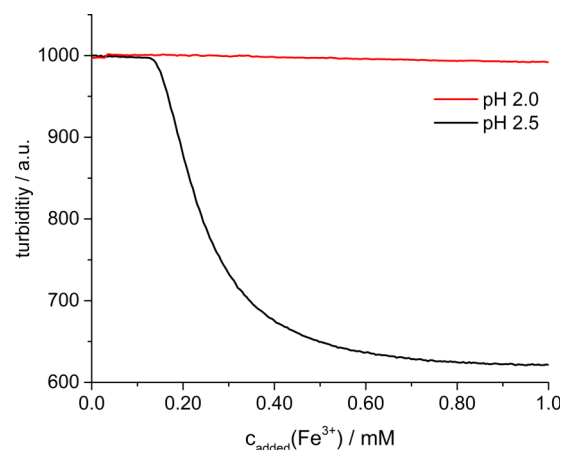


FIG. 3. Development of transmission in a solution containing  $0.05 \text{ g/l}$  pAsp ( $M_w = 3800 \text{ g/mol}$ ) at different pH values.

suggests that the mechanistic key step in precipitation is initiated essentially with the first addition of iron(III) ions. It can be concluded that the interactions between pAsp and hydrolyzed iron(III) species are progressively promoted. The latter have been demonstrated to qualify as PNCs, which are dynamic iron hydroxide colloid polymers.<sup>10</sup> Significant interactions between mononuclear, non-hydrolyzed iron(III) species, and the polyanion, on the other hand, do not occur and do not induce any precipitation. It is thus likely that the production of HCl that was observed by Lindén and Rabek<sup>23</sup> during iron(III) hydrolysis in the presence of PAA, and that was assigned to originate from PAA deprotonation upon adsorption of mononuclear aquo/chloro complexes to PAA chains, was also due to a promoted hydrolysis reactions of the iron(III) ions, since their experiments were carried out at pH values up to 7.

## B. Precipitate characterization

### 1. Size determination

The material that precipitated upon clouding was isolated and characterized with multiple analytical techniques. Additionally, the reaction solution was analyzed with different *in situ* analytics to provide insight into the structure and properties of the obtained precipitate in solution. Transmission electron microscopy (TEM), scanning electron microscopy (SEM), *in situ* atomic force microscopy (AFM) (Figure 4), light microscopy imaging (see Figure S5 of the [supplementary material](#)), and dynamic light scattering (DLS) (see Figure S6 of the [supplementary material](#)) revealed the presence of polydisperse spherical particles in a size range of 10 nm to the

$\mu\text{m}$  range. Generally, the particle sizes observed using electron microscopy were between 20 and 1  $\mu\text{m}$ , while the values determined with DLS (200 nm–1  $\mu\text{m}$ ) or light microscopy (1.5  $\mu\text{m}$ ) were somewhat smaller. In the case of the latter techniques, the resolution and contrast were insufficient for the detection of smaller particles and to determine whether the structures consist of aggregates, which are apparent in electron microscopy. It is therefore possible and likely that the large sizes detected with DLS, as well as the structures observed in the light microscope are in fact due to aggregates. Also, DLS is an *in situ* method while imaging with electron microscopy requires isolation of the particles, including a drying process. Aggregation was also observed by SEM, where the samples were freeze dried. TEM grids, in contrast, were prepared by placing a drop of the solution on the grid and letting it dry under ambient conditions. Drying effects can account for shrinking of the particles and thus explain the observation of smaller species on average by this technique. In the case of *in situ* AFM, the sample is not affected by drying effects, and particles in a size range of 10–70 nm are clearly observed (Figure 4(b)). We also observed that a few particles especially larger ones are not attached firmly on the mica surface and get removed by the tip during the scan (see Figure S7 of the [supplementary material](#)), which renders imaging of large precipitates (>100 nm) with AFM impossible. For *cryo*-TEM, drying effects are also absent as samples are prepared by rapid freezing in liquid ethane. In *cryo*-TEM images, larger composite particles up to 100 nm can be observed as well as aggregates of particles (Figure 6), supporting the abovementioned considerations. It has to be noted, however, that in *cryo*-TEM, the true diameter is difficult to determine due to the low contrast in frozen hydrated samples.

### 2. Composition of the material

*In situ* AFM analyses of the reaction solution on different surfaces indicate that the precipitate is positively charged: the precipitate was observed on bare mica surfaces, which are negatively charged, but no material was detected on mica that was modified to carry a positive surface charge using

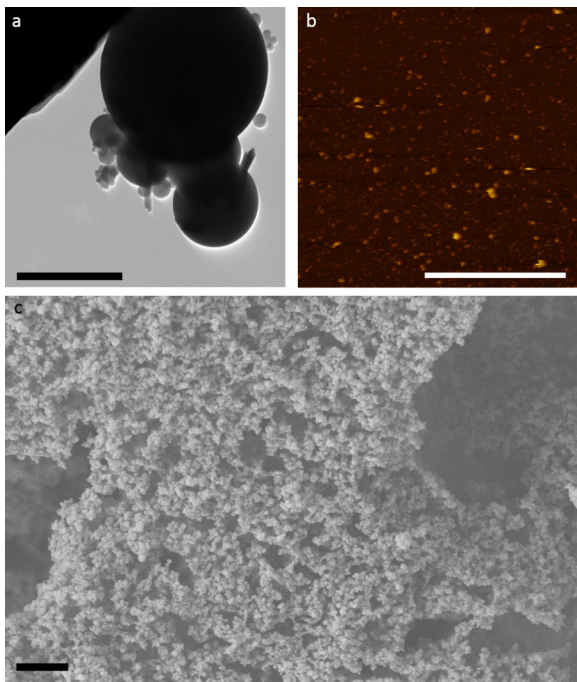


FIG. 4. (a) TEM image of a drop of the sample, dried on the TEM grid. (b) *In situ* AFM imaging of the reaction mixture. Particles with a size range of 10–70 nm are clearly observed. (c) SEM image of the isolated, freeze-dried material. All scale bars are 1  $\mu\text{m}$ .

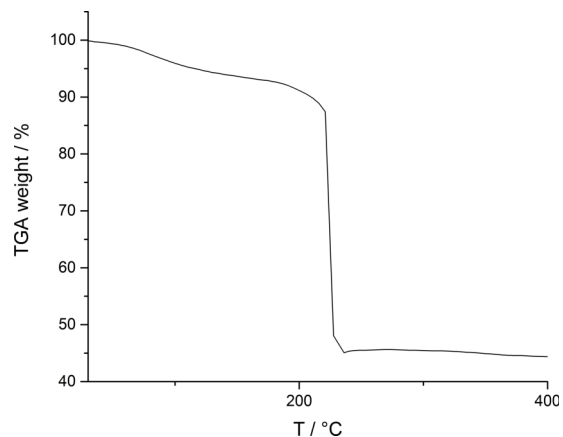


FIG. 5. TGA curve of the composite material isolated after 550 s from a titration carried out at pH 2.6.

poly-lysine (see Figure S8 of the [supplementary material](#)). This is consistent with zeta potential measurements, yielding  $17.1 (\pm 4.3)$  mV for the particles. *In situ* distance-force measurements give a Young's modulus of  $520.73 \pm 25.41$  kPa for the spheres. This value demonstrates that the deposited material is very soft, lying in the same range as nanocomposite gels,<sup>29</sup> diatom cells,<sup>30</sup> and human tissues,<sup>31</sup> and thus provides evidence for the presence of pAsp within the material (see Figure S9 of the [supplementary material](#)). This is further corroborated by thermogravimetric analysis, where the first observed weight loss at temperatures between 60 and 170 °C can be assigned to a water content of 6%-7% (Figure 5).

Degradation of the pAsp causes a relative weight loss of about 49% in a temperature range of 190–240 °C. This

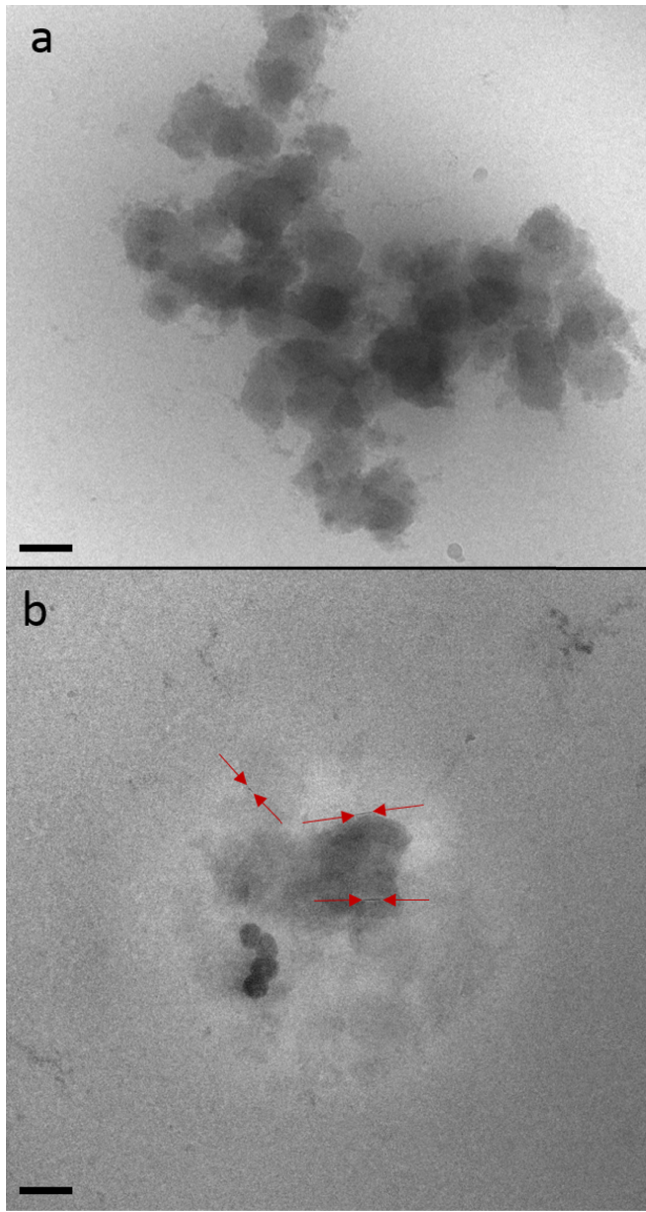


FIG. 6. Cryo-TEM images of partly hydrolyzed iron(III) salt in the presence of polyaspartic acid with a molecular weight of 3800 g/mol. The *in situ* technique shows similar features as seen in images obtained with SEM and TEM. Scale bar is 100 nm. Possibly crystalline needles can be observed in the sample (between red arrows in (b)).

reveals the high polymer content of the material, explaining its softness and shrinkage upon drying. Swelling experiments were conducted to determine whether the material can be classified as a gel. For that purpose, the sample, dried with a nitrogen stream, was examined by light microscopy and the size of selected particles or particle agglomerates were measured. Subsequently, a drop of water was placed on the sample and images were taken every half hour for 6 h.

It can be seen from the images and the size profiles prior to rehydration and after 6 h in water, that no measurable change in size occurs (see Figure S5 of the [supplementary material](#)) and hence, that the material is not a gel (there is no reversible swelling). Furthermore, crystallinity of the composite material was examined by X-ray diffraction, as in *cryo*-TEM images, needles and other seemingly crystalline particles can be observed (Figure 6). These crystals occur at stages of iron(III) hydrolysis at which in the absence of additive, only reversible olation and ligand exchange reactions take place (see Figure S1 of the [supplementary material](#)). The obtained diffraction pattern suggest an amorphous structure; however, crystallinity may be missed due to their small size and number. In any case, the formation of (potentially crystalline) particles is highly interesting as without additive at a comparable concentration, no precipitates are formed at all.

#### IV. CONCLUSION

The iron(III)-oxide-pAsp system represents another example for the distinct influence of a polymeric additive on particle formation<sup>13,32</sup> leading to the formation of a solid—composite—phase. The polydisperse particles formed in the presence of pAsp during the earliest stages of the hydrolysis reaction consist of both polymer and iron (oxyhydr)oxides and exhibit a slightly positive charge while being comparatively elastic and soft. However, the inability of the composite to reversibly swell and de-swell to larger and smaller sizes by rehydration and dehydration, all respectively, shows that the material is not a gel. Within the polydisperse composite material, iron (oxyhydr)oxide precipitates, which are potentially partially crystalline, are formed at very low iron concentrations of 0.4 mM at

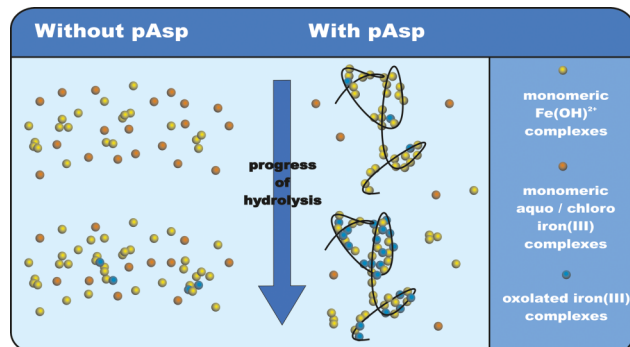


FIG. 7. Scheme illustrating the progression of hydrolysis in iron(III) systems without and in the presence of pAsp. With pAsp, the onset of oxolation, which is the molecular basis of the event of phase separation in the iron(III) (oxyhydr)oxide system,<sup>10</sup> can occur at much lower iron(III) concentrations and to a higher degree due to the adsorption of olation prenucleation clusters.

pH 2.5. Titration experiments shed light on the mechanisms underlying the additive effects. In non-hydrolyzed solutions at pH 2.0, the pAsp and the iron ions do not form any composite material nor does the hydroxide uptake increase in comparison to the reference experiments not containing polymer. Only in solutions possessing higher pH-values and therefore containing partly hydrolyzed olation PNCs,<sup>10</sup> the composite material forms. The hydroxide consumption cannot be rationalized with deprotonation of the polyacid and is thus assigned to a facilitated hydrolysis reaction. No precipitation at all is observed in the absence of the pAsp at these stages. The polymer promotes the hydrolysis and condensation of iron(III) (oxyhydr)oxide but does not induce these processes in non-hydrolyzed solutions. The interaction between pAsp and iron(III) olation pre-nucleation clusters at higher pH levels is unlikely to result from electrostatic interactions. The polymer chains barely carry any charge due to the low pH value, and the zeta potential of the composite material determined here lies in the same range as that of the PNCs in the system without additives.<sup>10</sup> The molecular weight of the pAsp has no significant effect besides the formation of more material when a larger molecular weight is used, but in presence of the monomeric L-aspartic acid, no precipitate is formed. This shows that the functional groups alone do not account for hydrolysis promotion and thus precipitation. In fact, the proximity and alignment of carboxyl functionalities along the polymer chains seem to be crucial for the observed effects.

It can be concluded that partly hydrolyzed olation PNCs<sup>10</sup> play a key role in the precipitation pathway of iron(III) (oxyhydr)oxides and explain the effects of pAsp based on PNC-pAsp interactions. We propose that the olation PNCs are adsorbed onto the pAsp, thereby facilitating the ongoing hydrolysis towards oxolation. We suggest that this is due to the close proximity and arrangement of the involved atoms, allowing for the occurrence of oxolation reactions within PNCs at significantly lower iron(III) concentrations than in additive-free scenario (Figure 7). Moreover, the adsorption of the olation PNCs on the pAsp chain prevents hydroxobridges from breaking, thus providing optimal conditions for promoting the onset of oxolation, which is the molecular basis of the phase separation event in this system.<sup>10</sup> Last but not least, it must be noted that the role of pAsp in iron(III)-oxide formation is fundamentally different from the case of calcium carbonate, where this additive is a strong inhibitor of nucleation and stabilizes liquid intermediates.<sup>12–15</sup> Polyanions that promote calcium carbonate formation, on the other hand, seem to rely on the segregation of single calcium ions,<sup>24</sup> as opposed to the cluster-based mechanism described here.

## SUPPLEMENTARY MATERIAL

See the [supplementary material](#) for additional titration data, swelling experiments, DLS, AFM images, and force distance measurements.

## ACKNOWLEDGMENTS

D.G. is a Research Fellow of the Zukunftskolleg of the University of Konstanz. We acknowledge the support by the Fonds der Chemischen Industrie and both the German Research Foundation (DFG) within Project No. GE 2278/6-1 and the National Science Foundation (NSF) under Grant No. DMR-1312697, which are part of the NSF-DFG “Materials World Network for Particle-mediated Control Over Crystallization: From the Pre-nucleation Stage to the Final Crystal.” We thank Jennifer Knaus for carrying out the TGA experiments.

- <sup>1</sup>U. Schwertmann and R. M. Cornell, “The iron oxides,” in *Iron Oxides in the Laboratory* (Wiley-VCH, Weinheim, 2007).
- <sup>2</sup>J. Baumgartner and D. Faivre, *Earth-Sci. Rev.* **150**, 520 (2015).
- <sup>3</sup>C. M. Flynn, *Chem. Rev.* **84**, 31 (1984).
- <sup>4</sup>J.-P. Jolivet, C. Chanéac, and E. Tronc, *Chem. Commun.* **2004**, 481.
- <sup>5</sup>H. Zhang, G. A. Waychunas, and J. F. Banfield, *J. Phys. Chem. B* **119**, 10630 (2015).
- <sup>6</sup>J. Baumgartner *et al.*, *Nat. Mater.* **12**, 310 (2013).
- <sup>7</sup>J. Dousma and P. L. de Bruyn, *J. Colloid Interface Sci.* **64**, 154 (1978).
- <sup>8</sup>W. Schneider, *Comments Inorg. Chem.* **3**, 205 (1984).
- <sup>9</sup>D. Gebauer *et al.*, *Chem. Soc. Rev.* **43**, 2348 (2014).
- <sup>10</sup>J. Scheck *et al.*, *J. Phys. Chem. Lett.* **7**, 3123 (2016).
- <sup>11</sup>C. J. Brinker and G. W. Scherer, in *Sol-Gel Science*, edited by C. J. B. W. Scherer (Academic Press, San Diego, 1990).
- <sup>12</sup>S. L. P. Wolf, K. Jähme, and D. Gebauer, *CrystEngComm* **17**, 6857 (2015).
- <sup>13</sup>A. Verch *et al.*, *Phys. Chem. Chem. Phys.* **13**, 16811 (2011).
- <sup>14</sup>L. B. Gower, *Chem. Rev.* **108**, 4551 (2008).
- <sup>15</sup>M. A. Bewernitz *et al.*, *Faraday Discuss.* **159**, 291 (2012).
- <sup>16</sup>R. M. Cornell, R. Giovanoli, and W. Schneider, *J. Chem. Technol. Biotechnol.* **46**, 115 (1989).
- <sup>17</sup>Y. Hu *et al.*, *Langmuir* **28**, 7737 (2012).
- <sup>18</sup>J. Dousma, T. J. Van den Hoven, and P. L. De Bruyn, *J. Inorg. Nucl. Chem.* **40**, 1089 (1978).
- <sup>19</sup>J. Scheck, T. Lemke, and D. Gebauer, *Minerals* **5**, 0524 (2015).
- <sup>20</sup>K. Kandori *et al.*, *J. Mater. Sci.* **27**, 719 (1992).
- <sup>21</sup>S. Musić *et al.*, *J. Colloid Interface Sci.* **160**, 479 (1993).
- <sup>22</sup>G. A. Norton *et al.*, *Environ. Sci. Technol.* **25**, 449 (1991).
- <sup>23</sup>L.-A. Lindén and J. F. Rabek, *J. Appl. Polym. Sci.* **50**, 1331 (1993).
- <sup>24</sup>P. J. M. Smeets *et al.*, *Nat. Mater.* **14**, 394 (2015).
- <sup>25</sup>R. M. Jones, *Mechanics of Composite Materials* (Scripta Book Company, Washington, D.C., 1975).
- <sup>26</sup>M. Siglreitmeier *et al.*, *Beilstein J. Nanotechnol.* **6**, 134 (2015).
- <sup>27</sup>M. Breulmann *et al.*, *Adv. Mater.* **10**, 237 (1998).
- <sup>28</sup>I. Ostolska and M. Wiśniewska, *Appl. Surf. Sci.* **311**, 734 (2014).
- <sup>29</sup>J. Araki, Y. Yamanaka, and K. Ohkawa, *Polym. J.* **44**, 713 (2012).
- <sup>30</sup>G. Francius *et al.*, *Environ. Microbiol.* **10**, 1344 (2008).
- <sup>31</sup>F. J. Carter *et al.*, *Med. Image Anal.* **5**, 231 (2001).
- <sup>32</sup>D. Gebauer *et al.*, *Adv. Mater.* **21**, 435 (2009).